Inorganic Chemistry

including bioinorganic chemistry

May 20, 2013
Volume 52, Number 10
pubs.acs.org/IC

Synthetic control and spectroscopic observation of the Robin–Day class II/III borderline

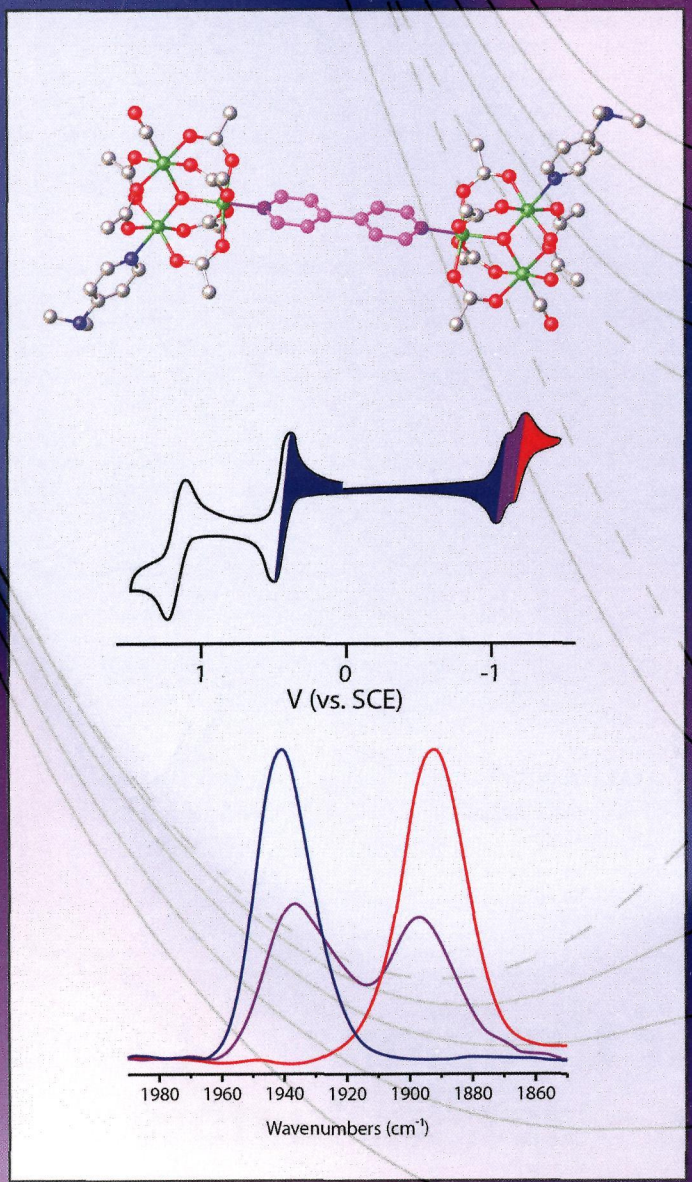

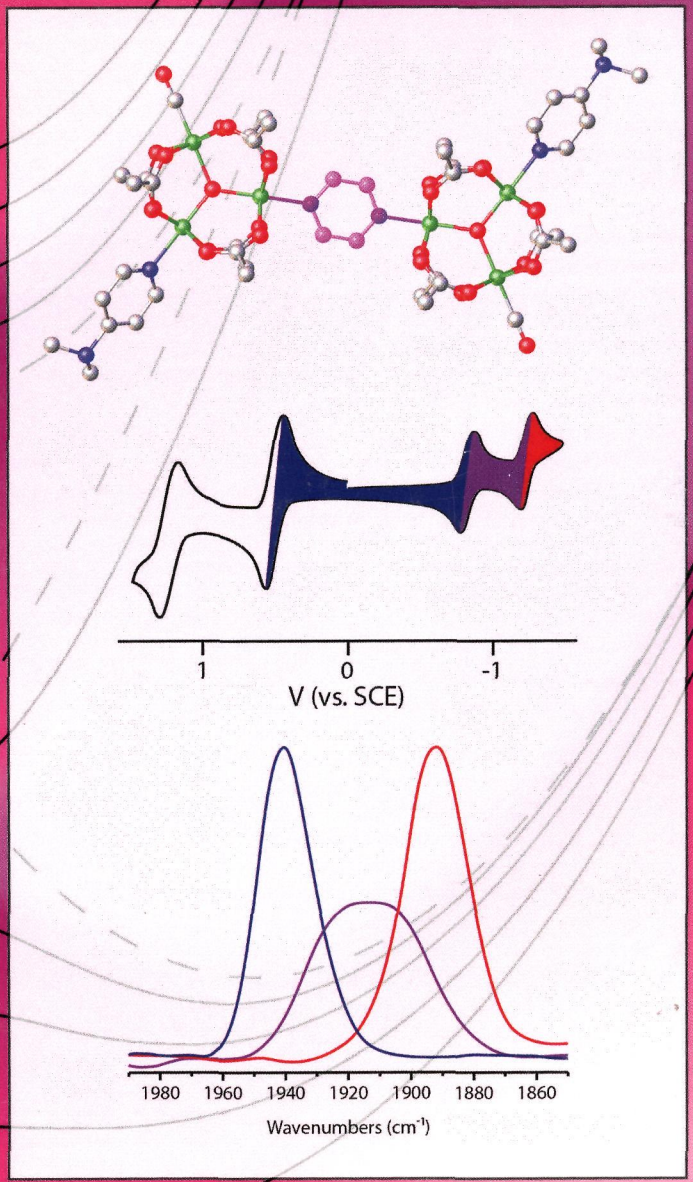

ACS Publications
MOST TRUSTED. MOST CITED. MOST READ.

www.acs.org

Inorganic Chemistry

MAY 20, 2013
VOLUME 52 ISSUE 10

INOCAJ 52(10) 5621−6232 (2013)
ISSN 0020-1669
Registered in the U.S. Patent and Trademark Office

ON THE COVER: An electronically tunable class of oxo-centered triruthenium dimer complexes is under exploration in the laboratory of Professor Clifford Kubiak. Electrochemical and IR spectroelectrochemical studies are used to probe the localized-to-delocalized transition in the mixed-valence states from an estimation of the electron-transfer rates on the picosecond timescale. See C. P. Kubiak, p 5663.

Communications

5627 S dx.doi.org/10.1021/ic400167w

Synthesis and Characterization of a "Pt_3Tl" Cluster Containing an Unprecedented Trigonal Environment for Thallium(I)

Úrsula Belío, Sara Fuertes, and Antonio Martín*

The tetranuclear $[\{Pt(CNC)(tht)\}_3Tl](PF_6)$ (tht = tetrahydrothiophene; SC_4H_8; CNC = *C,N,C*-2,6-$NC_5H_3(C_6H_4\text{-}2)_2$; **2**) cluster has been prepared and structurally characterized. The Tl^I atom is bonded to three Pt^{II} centers bearing a perfect trigonal coordination. The $Pt^{II}-Tl^I$ bonds are the shortest of this kind reported so far [2.9086(5) Å]. These intermetallic bonds persist in a CD_2Cl_2 solution, as shown by the $^{195}Pt\{^1H\}$ NMR spectrum of **2** at 193 K, in which a Pt−Tl coupling of 8.9 kHz is observed.

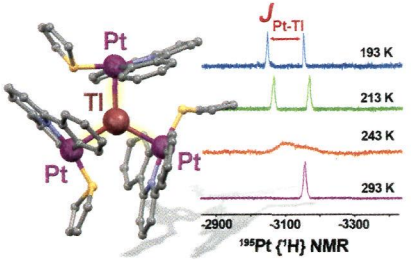

5630 S dx.doi.org/10.1021/ic400276c

Rational Synthesis of a Porous Copper(II) Coordination Polymer Bridged by Weak Lewis-Base Inorganic Monoanions Using an Anion-Mixing Method

Shin-ichiro Noro,* Katsuo Fukuhara, Yuh Hijikata, Kazuya Kubo, and Takayoshi Nakamura*

The use of divalent Cu^{II} ions and an anion-mixing method led to the rational construction of a porous coordination polymer bridged by weak Lewis-base inorganic $CF_3SO_3^-$ monoanions.

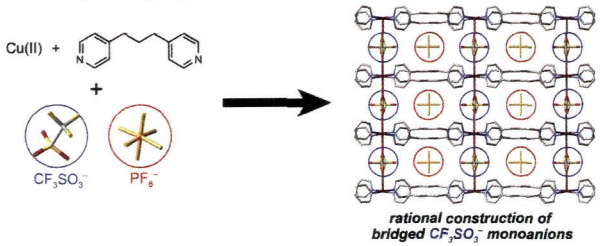

5633 S dx.doi.org/10.1021/ic400350w

dd Excitations in CPO-27-Ni Metal−Organic Framework: Comparison between Resonant Inelastic X-ray Scattering and UV−vis Spectroscopy

Erik Gallo, Carlo Lamberti,* and Pieter Glatzel*

We identify the dd excitations in the metal−organic framework CPO-27-Ni by coupling resonant inelastic X-ray scattering (RIXS) and UV−vis spectroscopies, and we show that the element selectivity of RIXS is crucial to revealing the full dd multiplet structure, which is not visible in UV−vis. The combination of calculations using crystal-field multiplet theory and density functional theory can reproduce the RIXS spectral features, crucially improving interpretation of the experimental data.

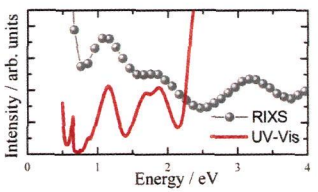

5636 S dx.doi.org/10.1021/ic400338v

A Terthiophene-Containing Alkynylplatinum Terpyridine Pacman Complex: Controllable Folding/Unfolding Modulated by Weak Intermolecular Interactions

Yang Cao, Michael O. Wolf,* and Brian O. Patrick

Folded and unfolded structures of a bimetallic alkynylplatinum terpyridine complex with a flexible terthiophene linker in both solution and the solid state are described. Weak intermolecular interactions stabilize the folded structure. In solution, folding is observed by electronic absorption spectroscopy and ^1H and NOESY NMR experiments.

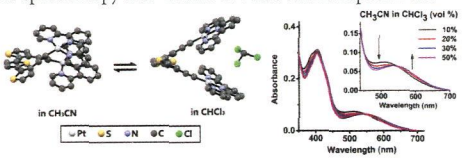

5639 S dx.doi.org/10.1021/ic4005505

Synthesis and Structure of a Carbene-Stabilized Boraallene Coordinated to Rhodium

Holger Braunschweig,* Qing Ye, and Krzysztof Radacki

Reaction of the (B,C-η^2)-1-aza-2-borabutatriene rhodium complex **1** with 1,3-dimethylimidazol-2-ylidene) (*I*Me, **2**) afforded the N-heterocyclic carbene-stabilized (C,C-η^2)-1-boraallene rhodium complex **3**, which has been characterized in solution and by X-ray crystallography. Density functional theory calculations were carried out to elucidate the observed base-induced B−C to C−C coordination mode shift, which suggested that the latter is 25 kJ/mol lower in energy.

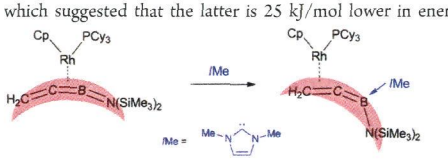

5642 S dx.doi.org/10.1021/ic4005938

Electronic Structural Changes of Mn in the Oxygen-Evolving Complex of Photosystem II during the Catalytic Cycle

Pieter Glatzel,* Henning Schroeder, Yulia Pushkar, Thaddeus Boron III, Shreya Mukherjee, George Christou, Vincent L. Pecoraro, Johannes Messinger, Vittal K. Yachandra,* Uwe Bergmann,* and Junko Yano*

Resonant inelastic X-ray scattering spectroscopy was used to study the oxygen-evolving complex in photosystem II in the intermediate states. The spectral changes during the transitions, compared to the changes in inorganic complexes, are subtle, indicating that the electrons are strongly delocalized throughout the cluster. The result suggests that, in addition to the Mn ions, ligands are playing an important role in the catalytic reaction. The results emphasize that the assignment of formal oxidation states alone is not sufficient for understanding the electronic tuning that governs the catalytic reaction.

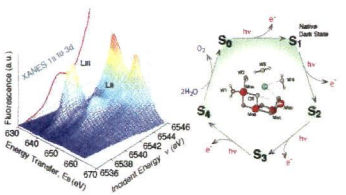

5645 S dx.doi.org/10.1021/ic400607w

Unique Coordination-Based Heterometallic Approach for the Stoichiometric Inclusion of High-Valent Metal Ions in a Porous Metal–Organic Framework

Keunil Hong, Woojeong Bak, and Hyungphil Chun*

A facile method for the stoichiometric inclusion of high-valent metal ions in a conventional metal(II) carboxylate metal–organic framework is introduced with an example of a Zn_3Ti system that possesses a permanent porosity and long-term stability.

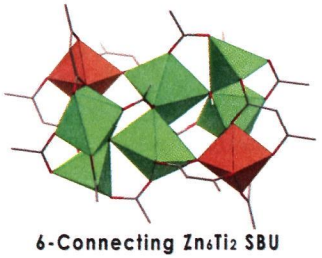

5648 S dx.doi.org/10.1021/ic400665m

Dodecanuclear Hexagonal-Prismatic $M_{12}L_{18}$ Coordination Cages by Subcomponent Self-assembly

Kiu-Chor Sham, Shek-Man Yiu, and Hoi-Lun Kwong*

Dodecanuclear hexagonal-prismatic $M_{12}L_{18}$ coordination cages were prepared by subcomponent self-assembly.

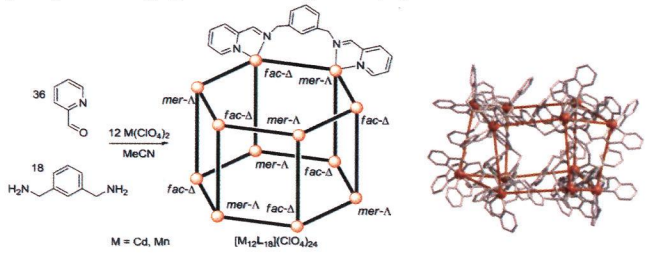

5651 S dx.doi.org/10.1021/ic400756z

Phosphorus(V) Complexes with Acyclic Monoaminocarbene Ligands via Oxidative Addition

Tobias Böttcher, Bassem S. Bassil, Lyuben Zhechkov, and Gerd-Volker Röschenthaler*

(Difluoroorganyl)dimethylamines, RCF_2NMe_2 (R = H, Ph, *t*Bu), can be used as carbene precursors for phosphorus trifluoride in an oxidative addition reaction. By this method, complexes of sterically nondemanding asymmetric and acyclic carbenes were obtained that are otherwise not accessible.

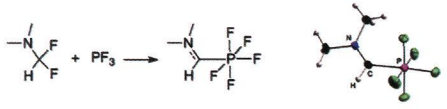

5654 S dx.doi.org/10.1021/ic4007795

Ionothermal Synthesis of Chiral Metal Phosphite Open Frameworks with In Situ Generated Organic Templates

Li-Ming Li, Kai Cheng, Fei Wang, and Jian Zhang*

Presented here is the ionothermal synthesis of two chiral quartz-type metal phosphite open frameworks containing in situ generated organic guests.

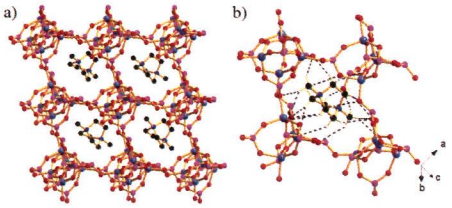

5657 S dx.doi.org/10.1021/ic400782c

Semiconducting $[(Bi_4Te_4Br_2)(Al_2Cl_{6-x}Br_x)]Cl_2$ and $[Bi_2Se_2Br](AlCl_4)$: Cationic Chalcogenide Frameworks from Lewis Acidic Ionic Liquids

Kanishka Biswas, In Chung, Jung-Hwan Song, Christos D. Malliakas, Arthur J. Freeman, and Mercouri G. Kanatzidis*

Cationic chalcogenide frameworks are rare, but they can be synthesized in organic ionic liquids containing strong Lewis acids such as $AlCl_3$. The Lewis acidic nature of the medium is believed to favor the assembly of the cationic chalcogenide $[Bi_2Q_2Br]^+$ frameworks.

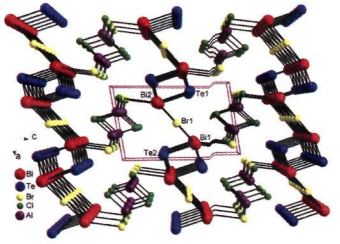

5660 S dx.doi.org/10.1021/ic400967k

A Trigonal-Prismatic Hexanuclear Technetium(II) Bromide Cluster: Solid-State Synthesis and Crystallographic and Electronic Structure

Erik V. Johnstone,* Daniel J. Grant, Frederic Poineau, Laura Fox, Paul M. Forster, Longzou Ma, Laura Gagliardi, Kenneth R. Czerwinski, and Alfred P. Sattelberger

$Na\{[Tc_6Br_{12}]_2Br\}$ was synthesized from the thermal decomposition of $TcBr_4$ under vacuum in a Pyrex glass ampule. The trigonal-prismatic $[Tc_6Br_{12}]$ cluster exhibits single Tc–Tc bonds along the triangular face and Tc≡Tc triple bonds along the edges. Density functional theory calculations were used to analyze the electronic and geometrical features of the $[Tc_6Br_{12}]$ cluster.

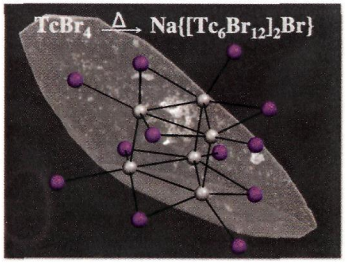

Award Paper

5663 dx.doi.org/10.1021/ic302331s

Inorganic Electron Transfer: Sharpening a Fuzzy Border in Mixed Valency and Extending Mixed Valency across Supramolecular Systems

Clifford P. Kubiak*

This article describes research from our laboratory on the chemistry and spectroscopic properties of inorganic mixed-valence complexes. After a brief review of the seminal work of Taube, Creutz, Day, Robin, Hush, and others in the 1960s and the confounding efforts to identify the borderline between class II and III mixed-valence systems in the 1990s and early 2000s, we describe our first experiments to observe and analyze the coalescence of ν(CO) band shapes in the 1D IR spectra of mixed-valence complexes of the type $\{[Ru_3O(OAc)_6(CO)(L)]_2\text{-BL}\}^-$, where L = a pyridyl ligand and BL = pyrazine or 4,4′-bipyridine, to estimate rate constants of intramolecular electron transfer.

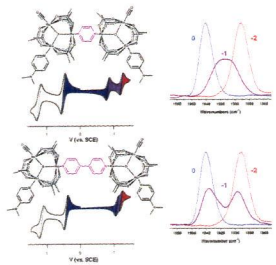

Articles

5677 dx.doi.org/10.1021/ic3012519

Differential Coordination Demands in Fe versus Mn Water-Soluble Cationic Metalloporphyrins Translate into Remarkably Different Aqueous Redox Chemistry and Biology

Artak Tovmasyan, Tin Weitner, Huaxin Sheng, MiaoMiao Lu, Zrinka Rajic, David S. Warner, Ivan Spasojevic, Julio S. Reboucas, Ludmil Benov,* and Ines Batinic-Haberle*

The profound difference between Fe and Mn porphyrins dominated by the differences in the thermodynamic properties, electron-deficiency of metal site, and steric and electrostatic factors impacts their biology as exemplified here with mouse data and with the differential protective effects on the aerobic growth of SOD-deficient *Escherichia coli*.

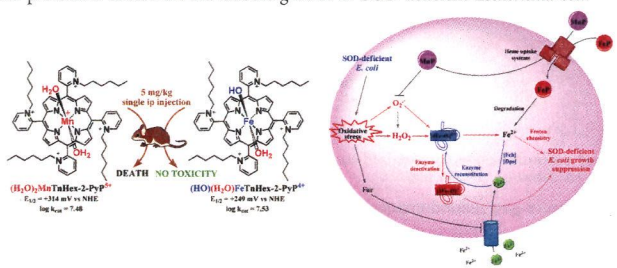

5692 dx.doi.org/10.1021/ic301810y

Evaluation of Multisite Polypyridyl Ligands as Platforms for the Synthesis of Rh/Zn, Rh/Pd, and Rh/Pt Heterometallic Complexes

Sarah K. Goforth, Richard C. Walroth, and Lisa McElwee-White*

Ligands containing dipicolylamine (dpa) and bipyridine (bpy) sites have been utilized in the synthesis of monometallic and heterobimetallic complexes. The two sites have different selectivities for metal binding, which allows preferential formation of singly metalated complexes. The dpa site of the ligands has been observed to bind selectively to Zn^{2+}, Pd^{2+}, and Pt^{2+} while the bpy site binds selectively to Rh^+. Addition of a second metal then results in the formation of heterometallic products.

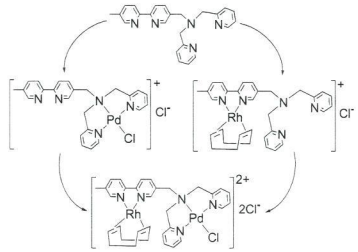

5702 dx.doi.org/10.1021/ic3022062

Computational Design of Two-Photon Fluorescent Probes for a Zinc Ion Based on a Salen Ligand

Shuang Huang, Lu-Yi Zou, Ai-Min Ren,* Jing-Fu Guo, Xiao-Ting Liu, Ji-Kang Feng, and Bao-Zhu Yang

Salen-based Zn^{2+} bioimaging reagents designed by an intramolecular charge-transfer mechanism were studied. The red shift of λ^{O}_{max} and λ^{EM}_{max} and the reduction of f upon coordination with Zn^{2+} reveal that they can be used for ratiometric detection. δ_{max} will decrease when the Salen ligand binds to Zn^{2+}, and most of the molecules exhibit a TPA peak in the near-infrared spectral region. A substituted position can influence the luminescence property, besides increasing solubility.

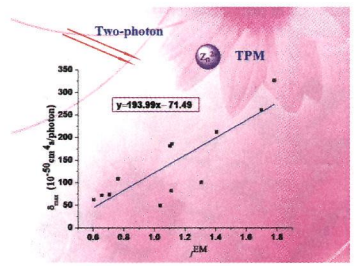

5714 dx.doi.org/10.1021/ic302355b

Heptacoordinated Molybdenum(VI) Complexes of Phenylenediamine Bis(phenolate): A Stable Molybdenum Amidophenoxide Radical

Mikko M. Hänninen, Petriina Paturi, Heikki M. Tuononen, Reijo Sillanpää, and Ari Lehtonen*

The reaction of noninnocent ligand precursor *N*,*N*′-bis(3,5-di-*tert*-butyl-2-hydroxyphenyl)-1,2-phenylenediamine ($H_4N_2O_2$) with $[MoO_2Cl_2(dmf)_2]$ yields heptacoordinated complex $[Mo(N_2O_2)Cl_2(dmf)]$, whereas the reaction with $[MoO_2(acac)_2]$ produces $[Mo(N_2O_2)(HN_2O_2)]$. Both complexes represent a rare case of molybdenum(VI) without any multiply bonded oxo or imido ligands. Molecular structures, magnetic measurements, ESR spectroscopy, and density functional theory calculations indicate that $[Mo(VI)(N_2O_2)(HN_2O_2)]$ is a stable molybdenum(VI) amidophenoxide radical.

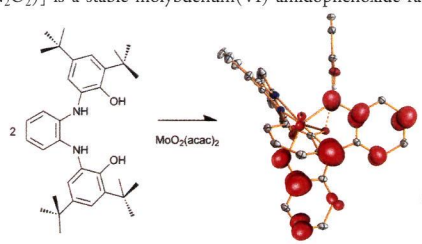

5722 dx.doi.org/10.1021/ic302395x

Bonding and Structure of Oxofluoroniobate-Based Glasses

Natalia M. Laptash,* Irina G. Maslennikova, Arseny B. Slobodyuk, Valery Ya. Kavun, and Vladimir K. Goncharuk

Chains of corner-sharing polyhedra with the preference to heteroatomic linkages and isolated $NbOF_5$ octahedra are the glass structural units in the systems K_2NbOF_5–MF_3 (M = Al, In). Fast reorientations of isolated $NbOF_5$ are reflected in the IR band at 700–800 cm^{-1} assigned to synchronous Nb–O and Nb–F stretching vibrations.

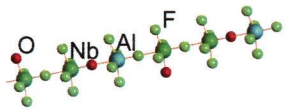

5729 dx.doi.org/10.1021/ic3024452

Novel Imino Thioether Complexes of Platinum(II): Synthesis, Structural Investigation, and Biological Activity

Paolo Sgarbossa, Silvia Mazzega Sbovata, Roberta Bertani, Mirto Mozzon, Franco Benetollo, Cristina Marzano, Valentina Gandin, and Rino A. Michelin*

We report the synthesis, characterization, and biological activity of the bis-imino thioether complexes *cis*-$[PtCl_2\{E\text{-}N(H)=C(SEt)R\}_2]$ (R = Me, Et, CH_2Ph, Ph) and *trans*-$[PtCl_2\{E\text{-}N(H)=C(SEt)R\}_2]$ (R = Me, Et, CH_2Ph, Ph), a series of new and effective cytotoxic agents.

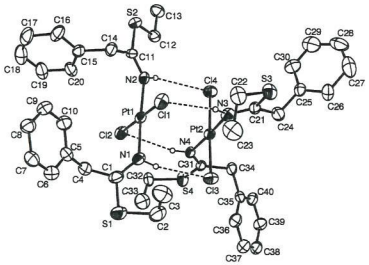

5742 dx.doi.org/10.1021/ic400924n

Role of the Electronically Excited-State Hydrogen Bonding and Water Clusters in the Luminescent Metal–Organic Framework

Xiao Sui, Min Ji, Xin Lan, Weihong Mi, Ce Hao,* and Jieshan Qiu

Through investigating the excited-state structures of four complexes Zn(3-tzba)(2,2′-bipy)(H_2O)·3H_2O, Zn(3-tzba)(2,2′-bipy)(H_2O)·2H_2O, Zn(3-tzba)-(2,2′-bipy)(H_2O)·H_2O, and Zn(3-tzba)(2,2′-bipy)(H_2O) (3-H_2tzba =3-(*SH*-tetrazolyl)benzoic acid), we have demonstrated that both the excited-state hydrogen bonding weakening and appropriate amount increasing of water molecules within the MOF should be in favor of the luminescence.

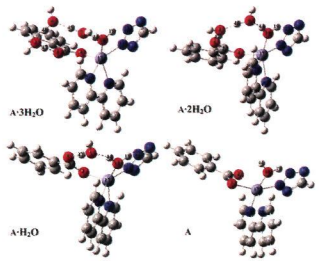

5749 dx.doi.org/10.1021/ic302552v

Noncovalent Interactions of Metal Cations and Arenes Probed with Thallium(I) Complexes

Titel Jurca, Ilia Korobkov, Serge I. Gorelsky,* and Darrin S. Richeson*

Thallium(I) complexes supported by the bis(imino)pyridine scaffold, $[\{ArN=CPh\}_2(NC_5H_3)]Tl^+(OTf)^-$, displayed cations with long Tl–N and Tl–OTf distances indicating weak ligand coordination, which was confirmed through computations. Additional intra- or intermolecular interactions between the Tl center and the arene rings were observed. In some cases inverted sandwich structures having two $[\{(2,5\text{-}^tBu_2C_6H_3)N=CPh\}_2(NC_5H_3)]Tl^+$ cations bridged by either benzene or toluene were obtained. A DFT description of these Tl-arene contacts required exchange-correlation functionals with long-range exchange corrections.

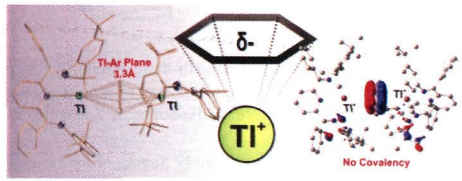

5757 dx.doi.org/10.1021/ic302557j

Exploring the Color of Transition Metal Ions in Irregular Coordination Geometries: New Colored Inorganic Oxides Based on the Spiroffite Structure, $Zn_{2-x}M_xTe_3O_8$ (M = Co, Ni, Cu)

S. Tamilarasan, Debajit Sarma, S. Bhattacharjee, U. V. Waghmare,* S. Natarajan, and J. Gopalakrishnan*

Spiroffite derivatives, $Zn_{2-x}M_xTe_3O_8$ (M^{II} = Co, Ni, Cu), featuring highly distorted octahedral Zn/MO_6 chromophores display brilliant colors (purple for M^{II} = Co, yellow for M^{II} = Ni and parrot green for M^{II} = Cu) that are different from the colors of the regular octahedral $Co^{II}O_6$, $Ni^{II}O_6$, Jahn–Teller distorted $Cu^{II}O_6$ chromophores. The unique colors of the spiroffite derivatives arise from the distortion of the Zn/MO_6 octahedra in the host structure, as revealed by optical absorption spectra and DFT electronic structure modeling.

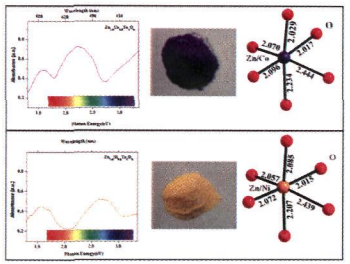

5764 dx.doi.org/10.1021/ic3025588

Magnetic Interactions Mediated by Diamagnetic Cations in $[Mn_{18}M]$ (M = Sr^{2+}, Y^{3+}, Cd^{2+}, and Lu^{3+}) Coordination Clusters

Ayuk M. Ako,* Boris Burger, Yanhua Lan, Valeriu Mereacre, Rodolphe Clérac,* Gernot Buth, Silvia Gómez-Coca, Eliseo Ruiz,* Christopher E. Anson, and Annie K. Powell*

A systematic survey of the effects of replacing the central Mn^{II} ion in the $[Mn_{19}]$ aggregate presenting a core corresponding to two supertetrahedral $\{Mn^{II}_4Mn^{III}_6\}$ units sharing a common Mn^{II} vertex, with various diamagnetic metal ions M^{n+} to afford $[Mn_{18}M]$ (M = Sr^{2+}, Y^{3+}, Cd^{2+}, and Lu^{3+}) clusters has been undertaken. Magnetic studies reveal that the diamagnetic metal cations are capable of mediating weak long-range antiferromagnetic interactions between the high spin ferromagnetically coupled subunits as corroborated by DFT calculations.

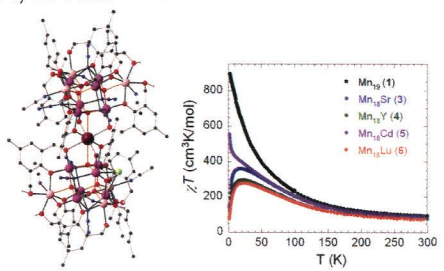

5775 S dx.doi.org/10.1021/ic3025843

Re and Br X-ray Absorption Near-Edge Structure Study of the Ground and Excited States of [ReBr(CO)$_3$(bpy)] Interpreted by DFT and TD-DFT Calculations

Stanislav Záliš,* Chris J. Milne,* Amal El Nahhas, Ana María Blanco-Rodríguez, Renske M. van der Veen, and Antonín Vlček Jr.*

Optical excitation of ReBr(CO)$_3$(bpy) to its lowest MLCT excited state is manifested in X-ray absorption spectra by the emergence of new pre-edge features in both Re L_3 and Br K spectral regions and by shifting both edges and the Re white line to higher energies. The XAS spectra and their changes upon excitation are well accounted for by TD-DFT calculations. The Re−Br delocalized origin of the excited electron is demonstrated both experimentally and theoretically.

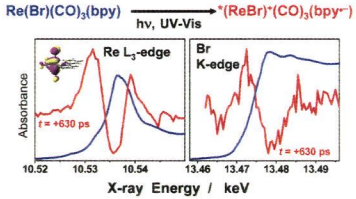

5786 S dx.doi.org/10.1021/ic302628y

Synthesis and Study of Three Novel Macrocyclic Selena[*n*]ferrocenophanes Containing a Naphthalene Unit

Wei Ji, Su Jing,* Zeyu Liu, Jing Shen, Jing Ma,* Dunru Zhu,* Dengke Cao, Limin Zheng, and Minxia Yao

Three macrocyclic selena[*n*]ferrocenophanes containing a naphthalene unit have been prepared. Upon complexation, electron density is withdrawn from the Se donor atoms, which leads to a significant energy shift in the HOMO level and large anodic shift of the half-wave potential of the 1,1′-ferrocenediyl group.

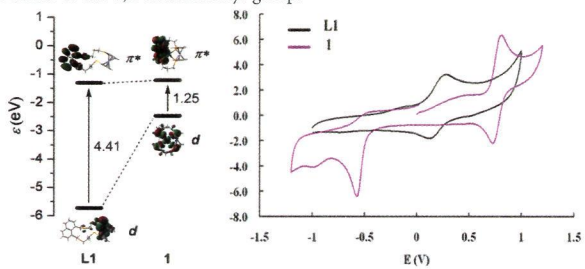

5794 dx.doi.org/10.1021/ic302629q

Photon-Driven Reduction of Zn^{2+} to Zn Metal

Anthony C. Brooks, Katherine Basore, and Stefan Bernhard*

Zinc metal is of interest as a means of storing solar energy in the form of fuels. In this vein, this work describes the photon driven reduction of Zn^{2+} by an iridium catalyst. A maximum of 430 catalyst turnovers are achieved in an optimized system with acetonitrile as the solvent. Kinetics measurements and cyclic voltammetry of Zn^{2+} salts are used to study the reaction mechanism.

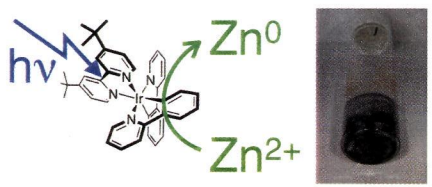

5801 S dx.doi.org/10.1021/ic302654s

Mechanism of the *cis*-[Pt(1*R*,2*R*-DACH)(H$_2$O)$_2$]$^{2+}$ Intrastrand Binding to the Double-Stranded (pGpG)·(CpC) Dinucleotide in Aqueous Solution: A Computational DFT Study

Zdeněk Chval,* Martin Kabeláč, and Jaroslav V. Burda*

A mechanism of the two-step intrastrand binding of the *cis*-[Pt(1*R*,2*R*-DACH)(H$_2$O)$_2$]$^{2+}$ complex to the double-stranded pGpG·CpC dinucleotide is studied in water solution by theoretical DFT methods. The reaction is kinetically preferred in the 5′ → 3′ direction since 5′ guanine is fully exposed to the solvent while the N7 center of 3′-guanine is sterically shielded. Structural, energetic, and electronic changes connected with the platinum complex binding to DNA are discussed in detail.

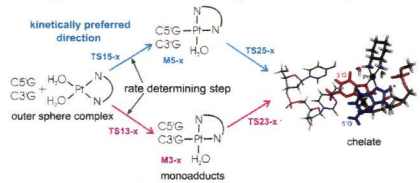

5814 S dx.doi.org/10.1021/ic400570h

Catalysis of Alkene Epoxidation by a Series of Gallium(III) Complexes with Neutral N-Donor Ligands

Wenchan Jiang, John D. Gorden, and Christian R. Goldsmith*

Six gallium(III) complexes with neutral N-donor ligands were prepared and used to catalyze the epoxidation of alkenes by peracetic acid. The use of more electron-deficient ligands increases the speeds and yields of the oxidations. The use of a higher denticity ligand increases the lifetime of the catalysis, although penta- and hexadentate ligands are associated with markedly decreased activity.

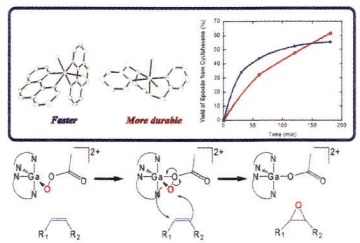

5824 S dx.doi.org/10.1021/ic3027545

Structural and Magnetic Characterization of a Tetranuclear Copper(II) Cubane Stabilized by Intramolecular Metal Cation−π Interactions

Raffaello Papadakis, Eric Rivière, Michel Giorgi, Hélène Jamet, Pierre Rousselot-Pailley, Marius Réglier, A. Jalila Simaan,* and Thierry Tron

A tetranuclear copper(II) complex displaying a cubane-type $Cu_4(OH)_4$ core was prepared. This complex seems to be stabilized by unusual metal cation−π interactions between the copper ions and phenyl substituents of the ligand. The tetranuclear complex is compared to a binuclear bis(μ-hydroxo)copper(II) complex and a mononuclear complex obtained using a similar ligand.

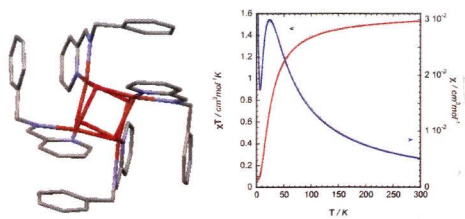

5831 S dx.doi.org/10.1021/ic302774h

$Cs_2GeB_4O_9$: a New Second-Order Nonlinear-Optical Crystal

Xiang Xu, Chun-Li Hu, Fang Kong, Jian-Han Zhang, Jiang-Gao Mao,* and Junliang Sun*

A new acentric alkali metal borogermanate, $Cs_2GeB_4O_9$ ($I\bar{4}$), has been discovered and a large crystal with dimensions of 20 × 16 × 8 mm^3 has been grown. It features a 3D anionic open framework based on interconnected GeO_4 tetrahedra and B_4O_9 clusters. $Cs_2GeB_4O_9$ exhibits a very high thermal stability with melt point of 849 °C, a short-wavelength absorption edge at 198 nm, and a strong SHG response of about 2.8 × KDP.

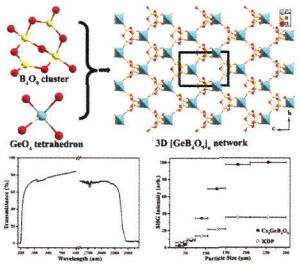

5838 S dx.doi.org/10.1021/ic302798u

Integrated and Passive 1,2,3-Triazolyl Groups in Fluorescent Indicators for Zinc(II) Ions: Thermodynamic and Kinetic Evaluations

J. Tyler Simmons, John R. Allen, Deborah R. Morris, Ronald J. Clark, Cathy W. Levenson,* Michael W. Davidson,* and Lei Zhu*

The thermodynamic and kinetic benefits of 1,2,3-triazolyl coordination in a multidentate ligand context are quantified via comparison of the properties of two isomeric ligands with integrated (coordinating) and passively (noncoordinating) attached 1,2,3-triazolyl groups, respectively. The 7-methoxycoumarin-containing ligand of the integrated design is an effective fluorescent indicator in imaging Zn ions in mammalian cells and rat hippocampal slices.

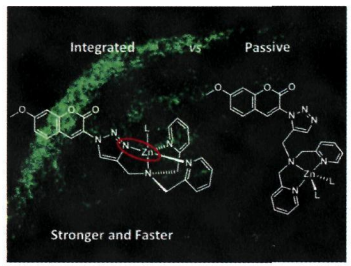

5851 S dx.doi.org/10.1021/ic3028012

Tris Chelating Phosphate Complexes of Bis(thio)urea Ligands

Rui Li, Yanxia Zhao, Shaoguang Li, Peiju Yang, Xiaojuan Huang, Xiao-Juan Yang, and Biao Wu*

Two bisurea and one bisthiourea ligands were synthesized, and their coordination properties with phosphate ion were studied. The ligands can readily coordinate to PO_4^{3-} ion to form the tris chelates $[(PO_4)L_3]^{3-}$ through 12 hydrogen bonds in the solid state. The coordination behavior in solution was also investigated.

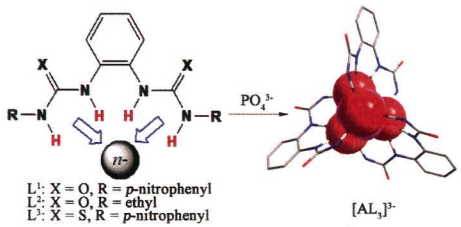

5861 S dx.doi.org/10.1021/ic302802h

Mixed Si/Ge Nine-Atom Zintl Clusters: ESI Mass Spectrometric Investigations and Single-Crystal Structure Determination of Paramagnetic $[Si_{9-x}Ge_x]^{3-}$

Markus Waibel and Thomas F. Fässler*

Dissolution of the ternary group 14 element Zintl phases $A_{12}Si_{17-x}Ge_x$ (A = K, Rb; x = 9, 12) in liquid ammonia led to the isolation of four $[E_9]^{3-}$ clusters with mixed Si and Ge site occupation. The existence of mixed clusters in solution was shown by ESI MS spectroscopy, and the paramagnetic nature was confirmed by EPR spectroscopy.

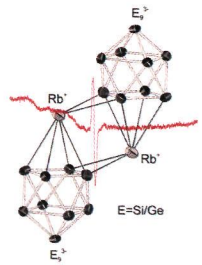

5867 S dx.doi.org/10.1021/ic302829e

Emissive Osmium(II) Complexes with Tetradentate Bis(pyridylpyrazolate) Chelates

Shih-Han Chang, Chun-Fu Chang, Jia-Ling Liao, Yun Chi,* Dong-Ying Zhou, Liang-Sheng Liao,* Tzung-Ying Jiang, Tsao-Pei Chou, Elise Y. Li,* Gene-Hsiang Lee, Ting-Yi Kuo, and Pi-Tai Chou

The osmium(II) metal phosphors with tetradentate bis(pyridylpyrazolate) chelates were synthesized, and their associated organic light-emitting diodes were fabricated, showing saturated red emission with a maximum external quantum efficiency (η_{ext}) of 9.8%.

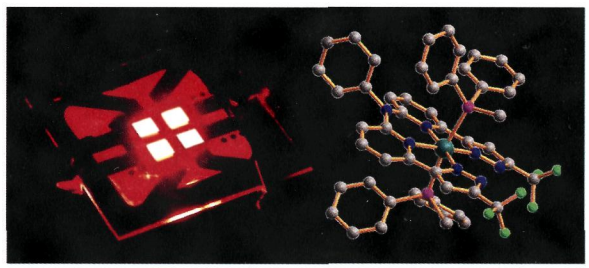

5876 S dx.doi.org/10.1021/ic302855f

General Strategy for the Synthesis of Rigid Weak-Link Approach Platinum(II) Complexes: Tweezers, Triple-Layer Complexes, and Macrocycles

Robert D. Kennedy, Charles W. Machan, C. Michael McGuirk, Mari S. Rosen, Charlotte L. Stern, Amy A. Sarjeant, and Chad A. Mirkin*

Rigid, *heteroligated* platinum(II)-based aryl–aryl′ weak-link approach (WLA) tweezer and triple-layer complexes have been synthesized using a partial chloride-abstraction method. Homoligated bisplatinum(II) WLA macrocycles have also been prepared using this strategy. The approach utilizes the halide-induced ligand rearrangement (HILR) reaction, and is general to hemilabile ligands of type $Ph_2PCH_2CH_2XAr$ (X = S, O, N). This work effectively brings the traditionally rhodium(I)-based chemistry of the WLA out of the glovebox and onto the bench.

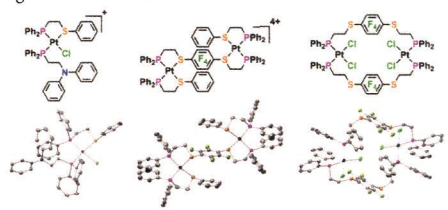

5889 dx.doi.org/10.1021/ic3028572

Solid State Molecular Device Based on a Rhenium(I) Polypyridyl Complex Immobilized on TiO_2 Films

Antonio Otavio T. Patrocinio, Karina P. M. Frin, and Neyde Y. Murakami Iha*

Photochemical and photophysical behaviors of *fac*-$[Re(CO)_3(phen)(trans\text{-}stpyCOOH)]^+$ adsorbed on TiO_2 have been investigated. The *trans*-to-*cis* photoisomerization ($\Phi = 0.23 \pm 0.03$) is the main process observed for the *trans*-isomer complex, both in solution and on a TiO_2 film. The *cis*-isomer complex is emissive in acetonitrile, but the radiative decay is quenched on the oxide surface by electron photoinjection to the device semiconductor. Both *trans*-to-*cis* ligand photoreaction and photoinjection of the immobilized Re(I) carbonyl complex can be conveniently applied to develop solid state photoswitches.

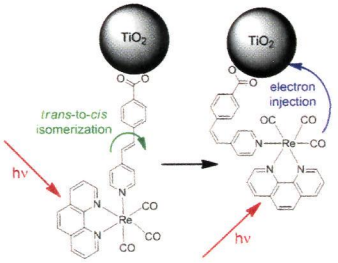

5897 dx.doi.org/10.1021/ic400037c

Enhanced Vapor-Phase Processing in Fluorinated Fe_4 Single-Molecule Magnets

Luca Rigamonti, Marco Piccioli, Luigi Malavolti, Lorenzo Poggini, Matteo Mannini, Federico Totti, Brunetto Cortigiani, Agnese Magnani, Roberta Sessoli,* and Andrea Cornia*

A new volatile single-molecule magnet $[Fe_4(L)_2(pta)_6]$ containing partially fluorinated β-diketonato ligands was assembled and shown to sublimate at temperatures as low as (440 ± 5) K (*Hpta* = pivaloyltrifluoroacetone, H_3L = 2-hydroxymethyl-2-phenyl-1,3-propandiol). According to XPS, ToF-SIMS, and ac susceptibility studies, the chemical composition, structure, and slow magnetic relaxation of the pristine material are fully retained in sublimated samples.

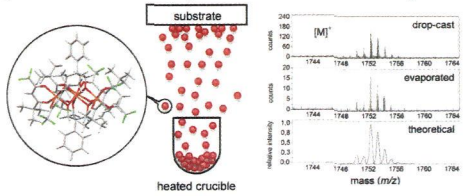

5906 dx.doi.org/10.1021/ic400053g

Reactivity of a Bis(amidinato)iron(II) Complex $[Fe(MesC(NPr^i)_2)_2]$ toward Some Oxidizing Reagents

Long Zhang, Li Xiang, Yihua Yu, and Liang Deng*

A diversified reactivity of the mononuclear bis(amidinato)iron(II) complex $[Fe(MesC(NPr^i)_2)_2]$ (**1**) toward oxidizing reagents has been disclosed. The bis(amidinato)iron(II) complex was synthesized from the reaction of $[Fe(Mes)_2]_2$ with 4 equiv of diisopropyl carbodiimide in good yield.

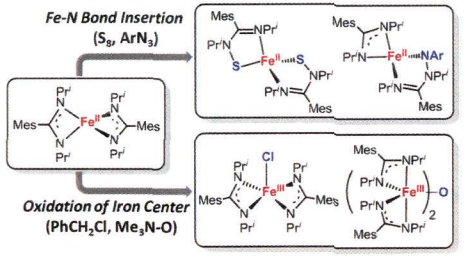

5914 dx.doi.org/10.1021/ic400055t

Well-Designed Strategy To Construct Helical Silver(I) Coordination Polymers from Flexible Unsymmetrical Bis(pyridyl) Ligands: Syntheses, Structures, and Properties

Zhu-Yan Zhang, Zhao-Peng Deng, Li-Hua Huo,* Hui Zhao, and Shan Gao*

A series of helical Ag(I) coordination polymers constructed from four flexible unsymmetrical bis(pyridyl) ligands have been synthesized under a well-designed strategy.

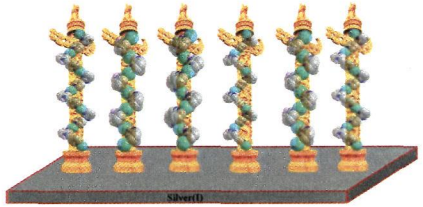

5924 dx.doi.org/10.1021/ic400109j

Porous Titania with Heavily Self-Doped Ti^{3+} for Specific Sensing of CO at Room Temperature

Juan Su, Xiao-Xin Zou,* Yong-Cun Zou, Guo-Dong Li, Pei-Pei Wang, and Jie-Sheng Chen*

We present a facile route to a heavily Ti^{3+} self-doped titania material, which serves as an efficient room-temperature gas-sensing material for specific CO detection. The self-dopant Ti^{3+} in titania proves to possess dual functions—decreasing the resistance of TiO_2 and increasing the chemisorbed oxygen species on the TiO_2 surface.

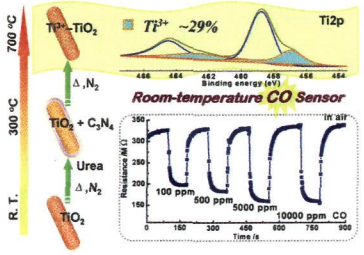

5931 dx.doi.org/10.1021/ic400145f

Molybdenum 17- and 18-Electron Bis- and Tris(Butadiene) Complexes: Electronic Structures, Spectroscopic Properties, and Oxidative Ligand Substitution Reactions

Gerald C. Stephan, Christian Näther, Gerhard Peters, and Felix Tuczek*

New results on the electronic structures, spectroscopic properties, and reactivities of the molybdenum tris(butadiene) and tris(2,3-dimethylbutadiene) complexes $[Mo(bd)_3]$ (1^{bd}) and $[Mo(dmbd)_3]$ (1^{dmbd}), respectively, are reported.

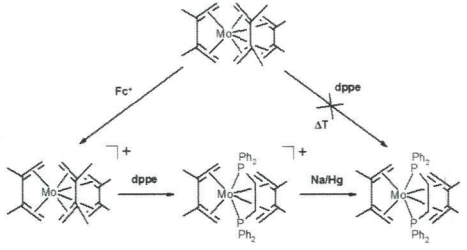

5943 (S) dx.doi.org/10.1021/ic400158q

Electrical Bistability around Room Temperature in an Unprecedented One-Dimensional Coordination Magnetic Polymer

Pilar Amo-Ochoa, Esther Delgado,* Carlos J. Gómez-García, Diego Hernández, Elisa Hernández, Avelino Martin, and Félix Zamora*

An unprecedented 1D coordination polymer containing $[Fe_2(S_2C_6H_2Cl_2)_4]^{2-}$ entities bridged by dicationic $[K_2(\mu\text{-}H_2O)_2(THF)_4]^{2+}$ shows pairwise Fe−Fe antiferromagnetic interactions and electrical bistability.

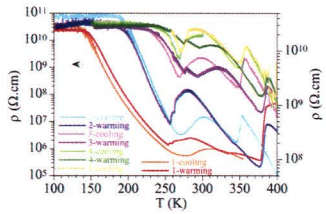

5951 (S) dx.doi.org/10.1021/ic400160d

Mono- and Polynuclear Copper(II) Complexes of Alloferons 1 with Point Mutations (H6A) and (H12A): Stability Structure and Cytotoxicity

Mariola Kuczer, Marta Błaszak, Elzbieta Czarniewska, Grzegorz Rosiński, and Teresa Kowalik-Jankowska*

Mononuclear and polynuclear copper(II) complexes of the alloferons 1 with the point mutations (H6A) $H^1GVSGA^6GQH^9GVH^{12}G$-COOH (Allo6A) and (H12A) $H^1GVSGH^6GQH^9GVA^{12}G$-COOH (Allo12A) have been studied by potentiometric, UV−visible, CD, EPR spectroscopic, and mass spectrometry (MS) methods. The biological results show that copper(II) ions *in vivo* did not cause any apparent apoptotic features. The most active was the Cu(II)−Allo12A complex formed at pH 7.4 with a $\{NH_2, N_{Im}\text{-}H^1, N_{Im}\text{-}H^6, N_{Im}\text{-}H^9\}$ binding site. It exhibited 123% higher caspase activity in comparison to that of Allo1.

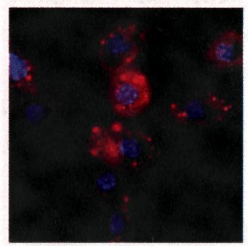

5962 (S) dx.doi.org/10.1021/ic4001957

Computational Study of the Initial Stage of Diborane Pyrolysis

Baili Sun and Michael L. McKee*

A schematic free energy diagram of $B_2H_6 + BH_3$ is shown. The rate-limiting step in the initial stage of diborane pyrolysis is the concerted formation and decomposition of B_3H_9.

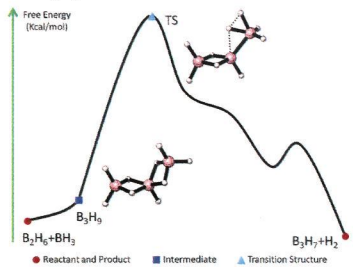

5970 (S) dx.doi.org/10.1021/ic400202r

Synthesis, Electrochemistry, and Reactivity of Cerium(III/IV) Methylene-Bis-Phenolate Complexes

Brian D. Mahoney, Nicholas A. Piro, Patrick J. Carroll, and Eric J. Schelter*

Methylene bis(phenolate) ligands are used to prepare a cerium(III) complex that exhibits a reversible electrochemical oxidation at $E_{1/2}$ = −0.93 V vs Fc/Fc^+ in THF. The properties of this reducing cerium(III) compound and its cerium(IV) oxidation products are examined through electrochemical and chemical means.

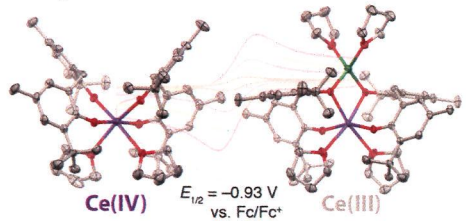

5978 (S) dx.doi.org/10.1021/ic400253m

A Series of Tetrathiafulvalene-Based Lanthanide Complexes Displaying Either Single Molecule Magnet or Luminescence—Direct Magnetic and Photo-Physical Correlations in the Ytterbium Analogue

Fabrice Pointillart,* Boris Le Guennic, Thomas Cauchy, Stéphane Golhen, Olivier Cador, Olivier Maury, and Lahcène Ouahab

The EDT-TTF core designed with two 2-pyridyl-*N*-oxidemethylthio arms (L^1) was used as antenna for NIR emission, which has been correlated to the dc magnetic data for the Yb^{III} complex. Change for the BMT-TTF core (L^2) has permitted the observation of SMM behavior for the Dy^{III} derivative due to the increasing of the energy gap between the ground and first excited states compared to the L^1-based equivalent.

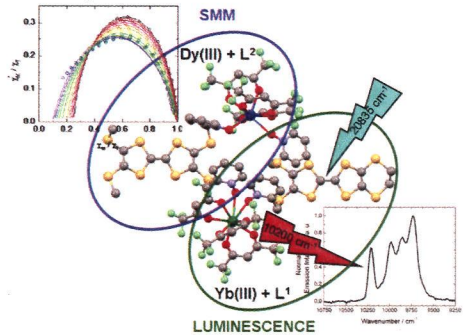

5991 (S) dx.doi.org/10.1021/ic400321k

Surface Modification of Al_{30} Keggin-Type Polyaluminum Molecular Clusters

Samangi Abeysinghe, Daniel K. Unruh, and Tori Z. Forbes*

Two model Al_{30} clusters, whose surface has been modified with chelated metals (Al^{3+} and Zn^{2+}) have been synthesized and structurally characterized by single-crystal X-ray diffraction to serve as model compounds for the adsorption of contaminants on aluminum-based adsorbents.

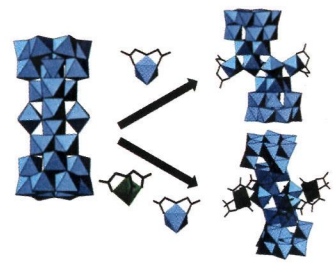

6000 S dx.doi.org/10.1021/ic400342m

Thermal Spin Crossover and LIESST Effect Observed in Complexes $[Fe(L^{Ch})_2(NCX)_2]$ [L^{Ch} = 2,5-Di(2-Pyridyl)-1,3,4-Chalcadiazole; Ch = O, S, Se; X = S, Se, BH_3]

Julia Klingele,* Dominic Kaase, Maximilian Schmucker, Yanhua Lan, Guillaume Chastanet, and Jean-François Létard

The LIESST and SCO behavior of five complexes belonging to the family of mononuclear $[Fe^{II}(L^{Ch})_2(NCX)_2]$ complexes has been investigated. A two-stepped T(LIESST) curve has been detected for $[Fe^{II}(L^{S})_2(NCS)_2]$. $[Fe^{II}(L^{Se})_2(NCS)_2]$ exhibits a small light induced thermal hysteresis (LITH), whereas no SCO could be detected for $[Fe^{II}(L^{O})_2(NCS)_2]$.

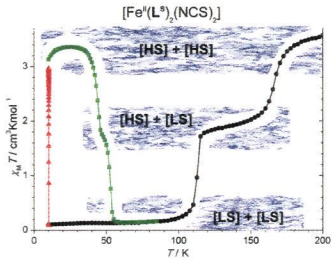

6011 S dx.doi.org/10.1021/ic400267s

Exploring a New Structure Family: Alkali Borosulfates $Na_5[B(SO_4)_4]$, $A_3[B(SO_4)_3]$ (A = K, Rb), $Li[B(SO_4)_2]$, and $Li[B(S_2O_7)_2]$

Michael Daub, Karolina Kazmierczak, Peter Gross, Henning Höppe,* and Harald Hillebrecht*

The topology of borosulfates depends on the ratio of BO_4 and SO_4 tetrahedra. Similar to the Si/O ratio in silicates, there are isolated units with a ratio of 1:4, chains with a ratio of 1:3, and a three-dimensional net with a ratio of 1:2.

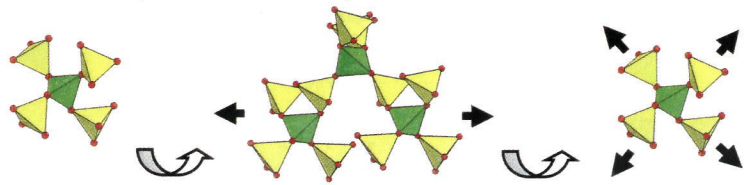

6021 S dx.doi.org/10.1021/ic400359x

Lanthanide Clusters with Azide Capping Ligands

Brian F. Moore, Thomas J. Emge, and John G. Brennan*

Weakly binding azide ligands have been used as surface caps in the synthesis of lanthanide oxo and selenido clusters. Attempts to prepare chalcogenido derivatives by ligand-based redox reactions using elemental Se were successful in the preparation of $(py)_{10}Er_6O_2(SeSe)_2(N_3)_{10}$, a diselenido cluster having crystallographic disorder due to some site sharing of both SeSe and N_3 ligands.

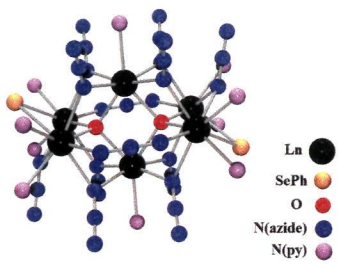

6028 dx.doi.org/10.1021/ic400382k

Revisiting the Spectroscopy of the Bi^{3+} Ion in Oxide Compounds

Philippe Boutinaud

A new model is introduced to account for the energy of metal-to-metal charge transfer transitions in oxide compounds containing Bi^{3+} ions and d^0 or d^{10} metals (M^{n+}). It is shown, through a critical review of the archival literature, that this model provides new insights on the assignment of the luminescence spectra and the related interpretation of the spectroscopic behaviors.

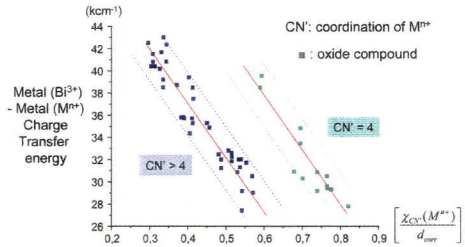

6039 S dx.doi.org/10.1021/ic400395n

High-Pressure Synthesis and Superconductivity of the Laves Phase Compound $Ca(Al,Si)_2$ Composed of Truncated Tetrahedral Cages $Ca@(Al,Si)_{12}$

Masashi Tanaka, Shuai Zhang, Kei Inumaru, and Shoji Yamanaka*

New ternary cubic Laves phase compounds $Ca(Al_{1-x}Si_x)_2$ ($0.35 \le x \le 0.75$) have been prepared under high-pressure and high-temperature conditions, which can be regarded as a new type of clathrate compound composed of face-sharing truncated tetrahedral cages with Ca atoms at the center, $Ca@(Al, Si)_{12}$. The compound with a stoichiometric composition CaAlSi exhibits superconductivity with T_c = 2.6 K. This is the first superconducting Laves phase compound composed solely of ubiquitous elements.

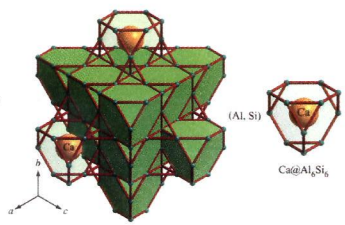

6046 S dx.doi.org/10.1021/ic400399v

Trans and Cis Influences in Hypervalent Iodine(III) Complexes: A DFT Study

P. K. Sajith and Cherumuttathu H. Suresh*

The trans and cis influences in acyclic and heterocyclic λ^3-iodanes have been quantified on the basis of I–OH bond distance (d), electron density at I–OH bond critical point (ρ), I–OH stretching frequency (ν), and molecular electrostatic potential minimum (V_{min}) at the OH lone pair. The interaction energies of Cl^- nucleophile in λ^3-iodanes have been rationalized using trans and cis influence parameters.

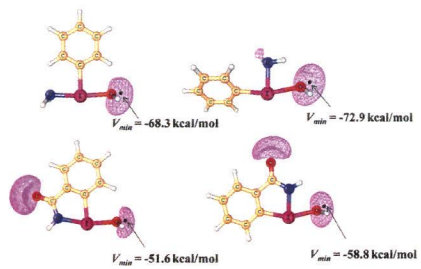

6055 S dx.doi.org/10.1021/ic4004017

3d Element Complexes of Pentadentate Bipyridine-Pyridine-Based Ligand Scaffolds: Structures and Photocatalytic Activities

Cyril Bachmann, Miguel Guttentag, Bernhard Spingler, and Roger Alberto*

The synthesis of the two penta-pyridyl type ligands pyridine-2,6-diylbis(dipyridin-2-ylmethanol) (PPy, **1**) and di-2,2′-bipyridin-6-yl(pyridin-2-yl)methanol (aPPy, **2**) is described. Both ligands coordinate rapidly to the 3d element cations Mn^{II}, Fe^{II}, Co^{II}, Ni^{II}, Cu^{II}, and Zn^{II}, thereby yielding complexes of the general composition $[MBr(\mathbf{1})]^+$ and $[MBr(\mathbf{2})]^+$, respectively. Further, the X-ray structures of selected complexes with ligands **1** and **2** are described. They show metal center dependent structural features and complexes with **2** exhibiting distinctly distorted octahedral geometries.

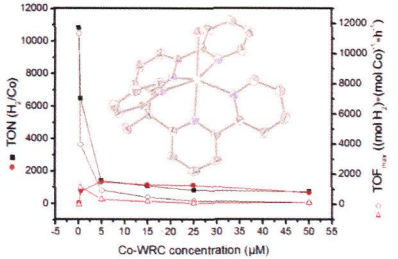

6062 S dx.doi.org/10.1021/ic400389d

Pyridinophane Platform for Stable Lanthanide(III) Complexation

Goretti Castro, Rufina Bastida, Alejandro Macías, Paulo Pérez-Lourido,* Carlos Platas-Iglesias,* and Laura Valencia

The solid state and solution structure and dynamics of Ln^{3+} complexes with a hexadentate pyridinophane ligand was investigated by using X-ray crystallography, ^1H and ^{13}C NMR in D^2O solution, and DFT calculations. A clear structural change occurring both in solution and in the solid state has been identified close to the middle of the lanthanide series at Sm^{3+}.

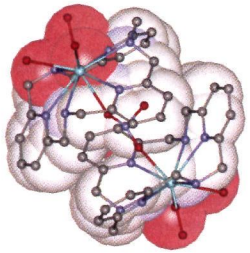

6073 S dx.doi.org/10.1021/ic400426m

Impact of Mn^{3+} upon Structure and Magnetism of the Perovskite Derivative $Pb_{2-x}Ba_xFeMnO_5$ ($x \sim 0.7$)

N. Barrier,* O. I. Lebedev, Md. Motin Seikh, F. Porcher, and B. Raveau

$Pb_{1.3}Ba_{0.7}MnFeO_5$ presents a perovskite derivative structure and is isostructural with $Pb_{2-x}Ba_xFe_2O_5$. The structural distortions due to the Mn^{3+}/Fe^{3+} substitution and the Jahn−Teller effect of Mn^{3+} were studied by powder neutron diffraction and high resolution electron microscopy/high angle annular dark field−scanning transmission electron microscopy. Here we show that the MO_6 octahedra of the double perovskite layers exhibit a strong tetragonal pyramidal distortion "5 + 1" and that the MO_5 polyhedra tend toward a tetragonal pyramid. $Pb_{1.3}Ba_{0.7}MnFeO_5$ exhibits a spin glass behavior with $T_g \sim 50$ K.

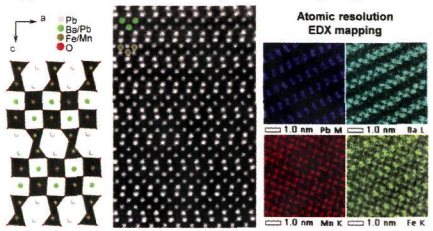

6083 S dx.doi.org/10.1021/ic400415h

Structure and Magnetic Properties of $Cu_3Ni_2SbO_6$ and $Cu_3Co_2SbO_6$ Delafossites with Honeycomb Lattices

J. H. Roudebush,* N. H. Andersen, R. Ramlau, V. O. Garlea, R. Toft-Petersen, P. Norby, R. Schneider, J. N. Hay, and R. J. Cava

The Delafossites with formula $Cu_3M_2SbO_6$ (M = Ni, Co) have been synthesized. Upon heat treatment close to the decomposition temperature, new Bragg reflections are observed in the powder diffraction patterns. Synchrotron X-ray diffraction and high resolution tunneling electron microscopy are used for characterization. The new reflections are indexed to a monoclinic cell which allows for the ordering of M and Sb atoms in a honeycomb lattice; in the Ni sample, an additional polytype is characterized.

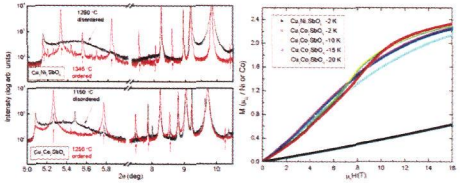

6096 S dx.doi.org/10.1021/ic400444u

Sr_2FeO_3 with Stacked Infinite Chains of FeO_4 Square Planes

Cédric Tassel, Liis Seinberg, Naoaki Hayashi, Subodh Ganesanpotti, Yoshitami Ajiro, Yoji Kobayashi, and Hiroshi Kageyama*

The synthesis of Sr_2FeO_3 through a hydride reduction of the Ruddlesden−Popper layered perovskite Sr_2FeO_4 is reported. Rietveld refinements using synchrotron and neutron powder diffraction data revealed that the structure contains corner-shared FeO_4 square-planar chains running along the [010] axis, being isostructural with Sr_2CuO_3 (*Immm* space group). Fairly strong Fe−O−Fe and Fe−Fe interactions along [010] and [100], respectively, make it an $S = 2$ quasi two-dimensional (2D) rectangular lattice antiferromagnet.

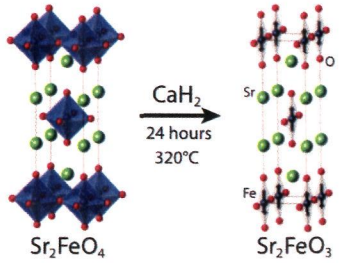

6103 S dx.doi.org/10.1021/ic400463a

Redox-Active Behavior of the [{Ti(η^5-C_5Me_5)(μ-NH)}$_3$(μ_3-N)] Metalloligand

Jorge Caballo, Jorge J. Carbó, Miguel Mena, Adrián Pérez-Redondo, Josep-M. Poblet, and Carlos Yélamos*

The reaction of $[K(C_5Me_5)]$ with the yttrium(III) adduct $[Cl_3Y\{(\mu_3\text{-}NH)_3Ti_3(\eta^5\text{-}C_5Me_5)_3(\mu_3\text{-}N)\}]$ occurs through an electron transfer to the titanium atoms while maintaining the yttrium center as trivalent. The potassium cation is retained in the resultant reduced specie but can be abstracted with crypt-222 to afford a well-separated ion pair $[K(crypt\text{-}222)][Cl_3Y\{(\mu_3\text{-}NH)_3Ti_3(\eta^5\text{-}C_5Me_5)_3(\mu_3\text{-}N)\}]$.

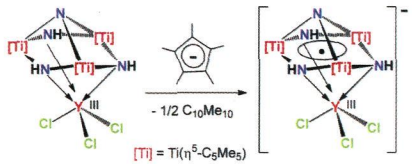

6110 S dx.doi.org/10.1021/ic400493v

Solid State Structure of $Bi(N_3)_3$, $Bi(N_3)_3$·Solvates and the Structural Dynamics in the $[Bi(N_3)_6]^{3-}$ Anion

Kati Rosenstengel, Axel Schulz,* and Alexander Villinger*

Utilizing a new solvothermal protocol, it was possible to isolate pure crystalline $Bi(N_3)_3$. Moreover, the lone pair activity in $[Bi(N_3)_6]^{3-}$ is discussed and chlorido-azido ligand back-exchange is demonstrated for bismuth azides.

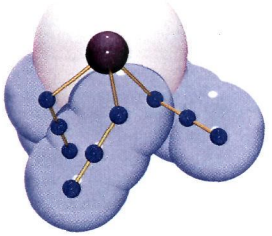

6127 S dx.doi.org/10.1021/ic400529s

Precession Electron Diffraction Tomography for Solving Complex Modulated Structures: the Case of $Bi_5Nb_3O_{15}$

Philippe Boullay,* Lukas Palatinus, and Nicolas Barrier

The crystal structure of the 1D incommensurately modulated phase $Bi_5Nb_3O_{15}$ is solved by electron diffraction using a tomography technique combined with precession of the electron beam. The present work shows how the electron density map, generated as an output of the charge-flipping structure solution procedure, can be interpreted to obtain a structural model even in such a complex case. The model is further validated by Rietveld refinement against powder X-ray diffraction data.

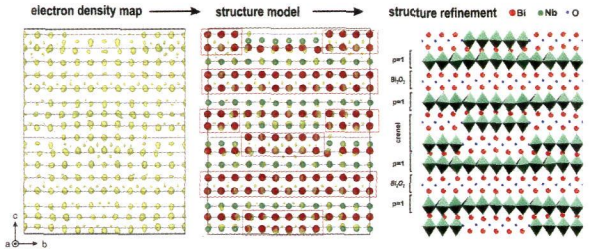

6136 S dx.doi.org/10.1021/ic400515m

$Sr_3BeB_6O_{13}$: A New Borate in the SrO/BeO/B_2O_3 System with Novel Tri-Six-Membered Ring $(BeB_6O_{15})^{10-}$ Building Block

Wenjiao Yao, Hongwei Huang, Jiyong Yao, Tao Xu, Xingxing Jiang, Zheshuai Lin,* and Chuangtian Chen

The modifications of the Be:B ratio in the SrO/BeO/B_2O_3 system successfully resulted in novel beryllium borates, which have greatly overcome the layering growth habit and structural polymorphism occurring in the two known compounds, $Sr_2Be_2B_2O_7$ and $SrBe_2B_2O_6$. Ultraviolet (UV)−visible−near-infrared diffuse reflectance spectroscopy and first-principles calculations reveal $Sr_3BeB_6O_{13}$ is transparent to the deep-UV region. This work may provide a new path to search for the deep UV crystals.

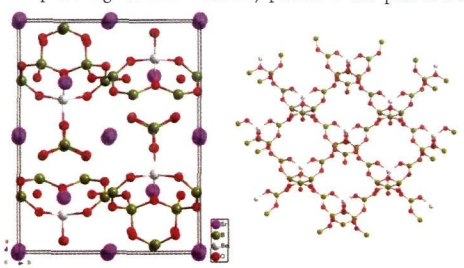

6142 S dx.doi.org/10.1021/ic400533u

Exploring the Scope of a Novel Ligand Class: Synthesis and Catalytic Examination of Metal Complexes with 'Normal' 1,2,3-Triazolylidene Ligands

Lars-Arne Schaper, Lilian Graser, Xuhui Wei, Rui Zhong, Karl Öfele, Alexander Pöthig, Mirza Cokoja, Bettina Bechlars, Wolfgang A. Herrmann,* and Fritz E. Kühn*

Using new 'normal'-substituted 1,2,3-triazolylidene silver compounds as starting materials allowed for preparation of a series of molybdenum, ruthenium, rhodium, and palladium transition metal complexes bound to the new 1,2,3-triazolylidene ligand system. In this work, the first triazolylidene Mo compound is presented as well as the first structural investigation of a silver complex with a monodentate 1,2,3-triazolylidene. Furthermore, the triazolylidene Pd complex and the Mo complex were tested as precatalysts in Suzuki−Miyaura coupling and epoxidation catalysis, respectively.

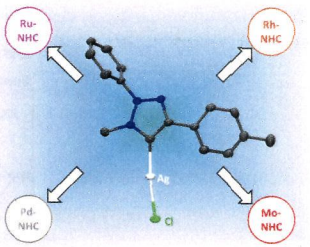

6153 S dx.doi.org/10.1021/ic400495w

Interaction between Platinum Complexes and the C-Terminal Motif of Human Copper Transporter 1

Erqiong Wang, Zhaoyong Xi, Yan Li, Lianzhi Li, Linhong Zhao, Guolin Ma,* and Yangzhong Liu*

Human copper transporter 1 (hCTR1) facilitates the cellular uptake of cisplatin, and the extracellular N-terminal domain has *been proven to coordinate to platinum drugs. Results show that the C8 peptide is highly reactive to cisplatin and oxaliplatin,* and the -HCH sequence is the most favorable binding site of platinum agents. These findings provide insight into the mechanism of the C-terminus of hCTR1 in the transfer of platinum drugs from the trimeric pore of hCTR1 to the cytoplasm.

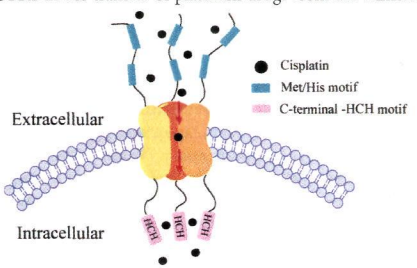

6160 S dx.doi.org/10.1021/ic400594u

Syntheses, Structures, and Magnetic Properties of Acetato- and Diphenolato-Bridged 3d–4f Binuclear Complexes [M(3-MeOsaltn)(MeOH)$_x$(ac)Ln(hfac)$_2$] (M = Zn^{II}, Cu^{II}, Ni^{II}, Co^{II}; Ln = La^{III}, Gd^{III}, Tb^{III}, Dy^{III}; 3-MeOsaltn = *N,N′*-Bis(3-methoxy-2-oxybenzylidene)-1,3-propanediaminato; ac = Acetato; hfac = Hexafluoroacetylacetonato; *x* = 0 or 1)

Masaaki Towatari, Koshiro Nishi, Takeshi Fujinami, Naohide Matsumoto,* Yukinari Sunatsuki, Masaaki Kojima, Naotaka Mochida, Takayuki Ishida, Nazzareno Re, and Jerzy Mrozinski

A series of 3d–4f binuclear complexes, [M(3-MeOsaltn)(MeOH)$_x$(ac)Ln(hfac)$_2$] (x = 0 for M = Cu^{II}, Zn^{II}; x = 1 for M = Co^{II}, Ni^{II}; Ln = Gd^{III}, Tb^{III}, Dy^{III}, La^{III}), have been synthesized. All complexes have an acetato- and diphenolato-bridged M^{II}–Ln^{III} binuclear structure. The magnetic interaction between M^{II} and Ln^{III} ions was investigated by an empirical approach based on a comparison of the magnetic properties of the M^{II}–Ln^{III}, Zn^{II}–Ln^{III}, and M^{II}–La^{III} complexes.

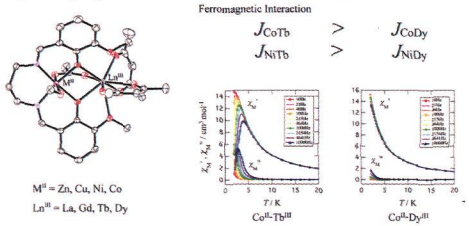

6179 S dx.doi.org/10.1021/ic400601n

Crystal Growth, Structure, Polarization, and Magnetic Properties of Cesium Vanadate, $Cs_2V_3O_8$: A Structure–Property Study

Jeongho Yeon, Athena S. Sefat, T. Thao Tran, P. Shiv Halasyamani, and Hans-Conrad zur Loye*

$Cs_2V_3O_8$ has been synthesized using a two-step hydrothermal technique. The material exhibits a two-dimensional layered crystal structure and belongs to the fresnoite structural family. Frequency-dependent polarization measurements indicated that $Cs_2V_3O_8$ is not a ferroelectric material. Magnetic property measurements revealed that $Cs_2V_3O_8$ can be considered a two-dimensional antiferromagnet.

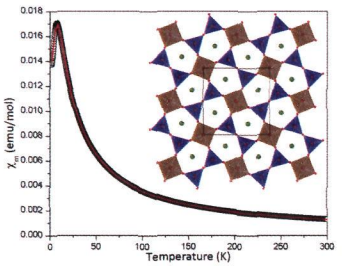

6187 S dx.doi.org/10.1021/ic400611z

Identifying Nanoscale M_{13} Clusters in the Solid State and Aqueous Solution: Vibrational Spectroscopy and Theoretical Studies

Milton N. Jackson Jr., Lindsay A. Wills, I-Ya Chang, Matthew E. Carnes, Lawrence F. Scatena, Paul Ha-Yeon Cheong,* and Darren W. Johnson*

Raman spectroscopy, infrared spectroscopy, and quantum mechanical computations were used to characterize and assign observed spectral features, highlight structural characteristics, and investigate the bonding environments of $[M_{13}(\mu_3\text{-}OH)_6(\mu_2\text{-}OH)_{18}(H_2O)_{24}](NO_3)_{15}$ (M = Al or Ga) nanoscale clusters in the solid phase and aqueous solution. Overall, each cluster has several unique vibrational modes in the low wavenumber region (< 1500 cm^{-1}) that are distinct from the parent nitrate salt and other polymeric species with similar structure, which allows for unambiguous identification of the cluster in solution and solid phases.

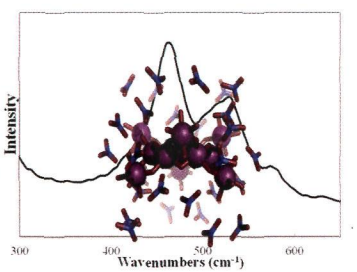

6193 S dx.doi.org/10.1021/ic400680r

Asymmetric Transfer Hydrogenation of Ketones Catalyzed by Enantiopure Osmium(II) Pybox Complexes

Esmeralda Vega, E. Lastra, and M. Pilar Gamasa*

The ^{i}Pr-pybox complexes *trans*-[OsCl$_2$(L){(*S,S*)-^{i}Pr-pybox}] (L = P(OMe)$_3$ (**1a**), P(OEt)$_3$ (**2a**), P(O^{i}Pr)$_3$ (**3a**), P(OPh)$_3$ (**4a**)) have proven to be active catalysts for the reduction of a variety of aromatic ketones providing enantioenriched alcohols with nearly complete conversion and high enantioselectivity (up to 94%). The efficiency of these catalysts depends not only on the chiral pybox but also on the nonchiral ligand L.

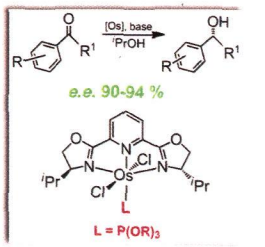

6199 S dx.doi.org/10.1021/ic400730a

POP-Pincer Osmium-Polyhydrides: Head-to-Head (*Z*)-Dimerization of Terminal Alkynes

Joaquín Alós, Tamara Bolaño, Miguel A. Esteruelas,* Montserrat Oliván, Enrique Oñate, and Marta Valencia

Two entries to obtain Os{xant(P^{i}Pr$_2$)$_2$} complexes, mainly polyhydrides, are described. Some of these compounds have the capacity for reducing H$^+$ and for promoting the head-to-head (*Z*)-dimerization of alkynes.

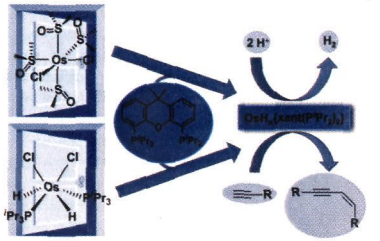

6214 S dx.doi.org/10.1021/ic400734t

Illustrating the Processability of Magnetic Layered Double Hydroxides: Layer-by-Layer Assembly of Magnetic Ultrathin Films

E. Coronado, C. Martí-Gastaldo,* E. Navarro-Moratalla, A. Ribera,* and S. Tatay

We report LbL fabrication of a magnetic hybrid organic–inorganic LDH/PSS UTF incorporating magnetic NiAl-LDH 2D nanosheets and PSS molecules. The UTF growth process has been monitored with FT-IR, UV–vis, and XRD, to confirm sequential deposition of bilayers and long-range order. Magnetic data confirms that the UTF and the bulk solid display equivalent magnetic behavior, thereby confirming the ability of exfoliated LDH nanosheets to retain the physical properties intrinsic to the macroscopic host and act as suitable vehicles to transfer these to more-complex architectures.

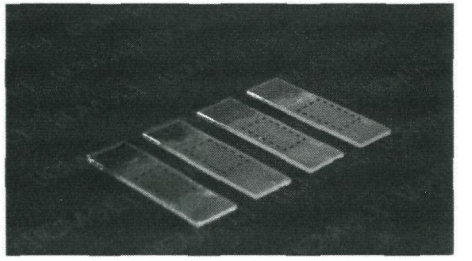

6223 Ⓢ dx.doi.org/10.1021/ic400786a

Click-Like Reactions with the Inert $HCB_{11}Cl_{11}^-$ Anion Lead to Carborane-Fused Heterocycles with Unusual Aromatic Character

James H. Wright II, Christos E. Kefalidis,* Fook S. Tham, Laurent Maron, and Vincent Lavallo*

The chlorinated carba-*closo*-dodecaborate anion $HCB_{11}Cl_{11}^-$ is an exceptionally stable molecule and has previously been reported to be substitutionally inert at the B–Cl vertices. We present here the discovery of base induced cycloaddition reactions between this carborane anion and organic azides that leads to selective C and B functionalization of the cluster. A single crystal X-ray diffraction study reveals bond lengths in the heterocyclic portion of the ring that are shortened, which suggests electronic delocalization.

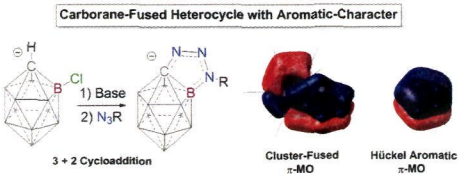

Additions and Corrections

6230 dx.doi.org/10.1021/ic401063b

Correction to First Ruthenium(II) Polypyridyl Complex As a True Molecular "Light Switch" for Triplex RNA Structure: $[Ru(phen)_2(mdpz)]^{2+}$ Enhances the Stability of Poly(U)·Poly(A)$_n$Poly(U)

Li-Feng Tan,* Jing Liu, Jian-Liang Shen, Xiao-hua Liu, Le-Li Zeng, and Lian-He Jin

6231 Ⓢ dx.doi.org/10.1021/ic401081m

Correction to 2,2′-Pyridylpyrrolide Ligand Redistribution Following Reduction

Keith Searles, Atanu K. Das, René W. Buell, Maren Pink, Chun-Hsing Chen, Kuntal Pal, David Gene Morgan, Daniel J. Mindiola, and Kenneth G. Caulton*

Ⓢ Supporting Information available via online article